Periodic orbit analysis of molecular vibrational spectra: Spectral patterns and dynamical bifurcations in Fermi resonant systems

Gregory S. Ezra

Baker Laboratory, Department of Chemistry, Cornell University, Ithaca, New York 14853

Semiclassical periodic orbit theory is used to analyze the quantum density of states for three model molecular vibrational Hamiltonians describing stretch/bend modes with and without 2:1 (Fermi) resonant coupling. Periods of classical periodic orbits as a function of energy are extracted directly from the quantum spectrum using a Gaussian windowed (Gabor) Fourier transform. The quantum (E,τ) plots so obtained provide an informative representation of the level structure. Qualitative similarities and differences between spectra (i.e., resonant vs nonresonant) are immediately apparent; in this sense, the quantum (E,τ) plot is an efficient device for analysis of spectral patterns. At a more detailed level of analysis, we show that, for sufficiently small effective values of $\hbar$, the quantum (E,τ) plots reflect in full detail the intricate periodic orbit bifurcation structure for Fermi resonant Hamiltonians previously described by Li, Xiao, and Kellman [J. Chem. Phys. **92**, 2251 (1990)]. © *1996 American Institute of Physics.* [S0021-9606(96)01101-X]

I. INTRODUCTION

Semiclassical periodic orbit (po) theory has been extensively applied over the last few years to explore the connection between classical and quantum mechanics for classically nonintegrable systems.[1,2] A central result of po theory is an approximate expression for the density of states in the semiclassical limit as a sum of terms, each associated with a periodic orbit of the system in the classical limit at the energy of interest.[1] Two limiting cases are well known. The Gutzwiller trace formula expresses the density of states as a sum over *isolated* pos, and is appropriate for the case of harsh chaos, where all pos are isolated and unstable.[1] The Gutzwiller trace formula also describes the contribution to the density of states from regions of phase space in the vicinity of isolated *stable* pos.[3] For integrable systems, the phase space is foliated by N-tori (for N degrees of freedom),[2] and the formula derived by Berry and Tabor gives the semiclassical density of states as a sum over rational *tori*.[4] Such rational tori, on which all N fundamental frequencies are commensurate, are covered by an $(N-1)$-dimensional family of pos.

A uniform semiclassical result describing the transition between the Gutzwiller and Berry–Tabor limits for the case of a resonant island chain has been derived by Ozorio de Almeida.[5]

Periodic orbit theory has been widely applied to *scaling* systems, i.e., those for which the classical phase space structure is the same for all values of the energy. Examples include the H atom in a magnetic field,[6] 3-body Coulomb systems[7,8] and quartic oscillators.[9]

Molecular vibrational Hamiltonians are prototypical examples of nonscaling systems. The vibrational phase space structure can change dramatically with energy, and the evolution of classical phase space structure with energy is indeed often of considerable interest.[10–13] Previous applications of semiclassical po theory to molecular spectra have mainly addressed qualitative issues of wave function

localization.[12] Periodic orbits and their bifurcations also form the basis of Kellman's approach to the analysis of resonantly coupled modes, in which a systematic study is made of bifurcations on the polyad phase sphere.[10]

A key to the more systematic application of po theory to vibrational spectra is the introduction of a window function in energy prior to Fourier transformation of the density of states. The use of window functions is familiar in the analysis of nonstationary signals in the time domain.[14] For example, local frequency analysis of irregular trajectories provides considerable insight into pathways for exploration of phase space in multimode systems.[15] Use of a window function enables one to explore the evolution of po periods with energy using quantum (E,τ) plots, and to identify signatures of classical bifurcations (see below). Johnson and Kinsey used a Blackman–Harris window[16] to analyze oscillatory structure in the absorption spectrum of O_3.[17] Baranger *et al.* introduced the use of a Gaussian window, the Gabor[14] or Husimi[18] transform, and computed classical and quantum (E,τ) plots for a number of potentials.[19] Rouben and Ezra have recently examined in some detail the bifurcation associated with the local to normal mode transition in a system of two 1:1 resonantly coupled anharmonic oscillators.[20] Other recent work on this problem includes the "vibrogram" analysis of Liévin *et al.*[21] and of Gaspard, Hirai, and Heller,[22] and the closely related studies of O'Connor and Kellman.[23]

The importance of recognizing and analyzing characteristic spectral patterns in strongly coupled systems has been stressed by Svitak *et al.*, who examined level spacing patterns in Fermi resonant systems.[24] Differences between level spacing patterns within polyads associated with the presence or absence of a separatrix were noted.[24]

In this paper we apply the Gabor transform method to compute quantum (E,τ) (po energy vs period) plots for vibrational level spectra of Fermi resonant systems of the type studied by Kellman and co-workers.[25–27] These systems

have been shown to have a rich and complex phase space structure.[25] Each vibrational polyad can be located in one of four "zones" representing a distinct kind of phase space morphology, and the system can pass from one zone to another by variation of parameters such as coupling strengths and polyad number.[26,27]

Our po analysis of the Fermi resonant systems yields two main results. First of all, at the most qualitative level, the quantum (E,τ) plots immediately enable one to distinguish between the spectra computed using two different Hamiltonians, one "diagonal" and the other "resonant," which were used to fit a target spectrum, itself obtained using a slightly more complicated resonant Hamiltonian.[24] Moreover, the quantum (E,τ) plots for the resonant and target spectra are very similar, showing the clear superiority of the resonant fitting Hamiltonian to the diagonal version. In this sense, the po analysis can be thought of as a generalized spectral pattern recognition tool, which analyzes local (in energy) oscillations in the level density.

At a more refined level of analysis, we find a remarkable correspondence between quantum (E,τ) plots for Fermi resonant systems and the periodic orbit structure on the polyad phase sphere. In particular, we can recognize the characteristic signatures in the (E,τ) plots of the distinct zones defined by Xiao and Kellman,[26,27] and are able to identify the bifurcations associated with transitions between zones. In this way we are able to follow a system as it passes (with increasing energy) from zone to zone.

This paper is organized as follows. In Sec. II we describe the classical and quantum mechanical Hamiltonians for the Fermi resonant systems to be studied. Section III surveys the classical phase space structure for the Fermi resonant systems, following the polyad phase sphere analysis of Kellman. In Sec. IV we briefly review the periodic orbit analysis of the density of states for nonscaling systems. Section V gives the results of our po analysis, and concluding remarks are given in Sec. VI.

II. MODEL HAMILTONIAN FOR FERMI RESONANT SYSTEM

The Hamiltonian studied in the present paper describes a single stretching vibration coupled to a doubly degenerate bending mode. An important example is the coupling of the CH bond stretch to the HCX bend in HCX_3 molecules.[28] The frequency of the stretching mode in such molecules is often approximately twice that of the bend, so that 2:1 resonant coupling terms can lead to strong mode mixing.

A. Quantum Hamiltonian

There are three relevant quantum numbers in the uncoupled system: n_s, the number of stretching quanta, n_b, the total number of bending quanta, and l, the vibrational angular momentum, where $l = n_b, n_b-2, n_b-4,...1$ or 0. We shall work in the $l=0$ subspace (n_b even) throughout, and so label basis states with two quantum numbers only: $|n_s, n_b\rangle$. In terms of these quantum numbers, the most general form of the diagonal part of the Hamiltonian we shall use is

$$\hat{H}^0 = \hat{H}_2^0 + \hat{H}_3^0 + \hat{H}_4^0, \tag{2.1}$$

with[24]

$$\hat{H}_2^0 = \omega_s(n_s+\tfrac{1}{2}) + \omega_b(n_b+1) + X_{ss}(n_s+\tfrac{1}{2})^2 + X_{sb}(n_s+\tfrac{1}{2})$$
$$\times (n_b+1) + X_{bb}(n_b+1)^2, \tag{2.2}$$

$$\hat{H}_3^0 = X_{sss}[(n_s+\tfrac{1}{2})^3 - \tfrac{1}{8}] + X_{ssb}[(n_s+\tfrac{1}{2})^2(n_b+1) - \tfrac{1}{4}]$$
$$+ X_{sbb}[(n_s+\tfrac{1}{2})(n_b+1)^2 - \tfrac{1}{2}] + X_{bbb}[(n_b+1)^3 - 1], \tag{2.3}$$

$$\hat{H}_4^0 = X_{ssss}[(n_s+\tfrac{1}{2})^4 - 1/16] + X_{sssb}[(n_s+\tfrac{1}{2})^3(n_b+1) - \tfrac{1}{8}]$$
$$+ X_{ssbb}[(n_s+\tfrac{1}{2})^2(n_b+1)^2 - \tfrac{1}{4}] + X_{sbbb}[(n_s+\tfrac{1}{2})$$
$$\times (n_b+1)^3 - \tfrac{1}{2}] + X_{bbbb}[(n_b+1)^4 - 1]. \tag{2.4}$$

In a basis of eigenstates of the zeroth-order Hamiltonian $\hat{H}^0$, $|n_s, n_b\rangle$, the nonzero matrix elements of the 2:1 resonant coupling $\hat{V}_{2:1}$ are[28]

$$\langle n_s, n_b | \hat{V}_{2:1} | n_s-1, n_b+2 \rangle = (-) \frac{k_{sbb}}{2}(n_b+2)\sqrt{\frac{n_s}{2}}. \tag{2.5}$$

That is, the coupling $\hat{V}_{2:1}$ is the resonant part of the operator

$$\hat{V} = k_{sbb}\hat{q}_s\hat{q}_b^2, \tag{2.6}$$

where, in terms of the degenerate bending normal mode coordinates $\hat{q}_{bx}$ and $\hat{q}_{by}$, $\hat{q}_b^2 = \hat{q}_{bx}^2 + \hat{q}_{by}^2$.[28,29]

The quantum Hamiltonian

$$\hat{H} = \hat{H}^0 + \hat{V}_{2:1} \tag{2.7}$$

is diagonal in the quantity $P = n_s + (n_b/2)$, so that together with the energy there are two integrals of the motion. Diagonalization of the quantum Hamiltonian in the basis $|n_s, n_b\rangle$ gives the quantum level spectrum. Because of the conservation of P, we are able to diagonalize matrices corresponding to each *polyad* independently, where a polyad is defined by a particular integer (or half-integer) value of P.

Parameter values for the three Hamiltonians studied in the present paper are given in Table I. These Hamiltonians were studied by Svitak *et al.*:[24] $\hat{H}^{sim}$, a general Fermi resonant Hamiltonian containing terms up to quartic in action; $\hat{H}^{res}$, a resonant Hamiltonian with quadratic $\hat{H}^0$ and parameters determined by fitting the spectrum of $\hat{H}^{sim}$; $\hat{H}^{diag}$, a diagonal Hamiltonian ($k_{sbb}=0$) including terms up to cubic in action, with parameters chosen to give the best (least-squares) fit to the spectrum of $\hat{H}^{sim}$. The parameters of Table I correspond to taking $\hbar=1$, so that, for a given integer polyad number P, there are $P+1$ states in the polyad. The quantum density of states at a given classical energy E can be multiplied by a factor c by scaling the Hamiltonian parameters as follows:

$$\omega_s \rightarrow \omega_s c^{-1}, \qquad \omega_b \rightarrow \omega_b c^{-1}; \tag{2.8a}$$

$$X_{ss} \rightarrow X_{ss}c^{-2}, \qquad X_{sb} \rightarrow X_{sb}c^{-2}, \qquad X_{bb} \rightarrow X_{bb}c^{-2}, \tag{2.8b}$$

$$X_{sss} \rightarrow X_{sss}c^{-3}, ..., \tag{2.8c}$$

TABLE I. Parameters for Fermi stretch–bend Hamiltonians.

	$\hat{H}^{\text{sim}}$	$\hat{H}^{\text{res}}$	$\hat{H}^{\text{diag}}$
$\omega_s{}^{\text{a}}$	3113.70	3121.18	3143.97
ω_b	0.444 67	0.437 6	0.428 75
X_{ss}	−0.018 27	−0.019 00	−0.026 92
X_{sb}	−0.004 496 3	−0.004 588	0.003 464
X_{bb}	−0.000 102 8	−0.000 195	0.000 384 9
X_{sss}	$3.693\ 4\times10^{-6}$	0.000	0.002 061
X_{ssb}	−0.000 011 24	0.000	−0.001 132
X_{sbb}	$-1.637\ 9\times10^{-7}$	0.000	−0.000 862
X_{bbb}	−0.000 012 08	0.000	−0.000 051
X_{ssss}	$3.693\ 4\times10^{-7}$	0.000	0.000
X_{sssb}	$-8.671\ 4\times10^{-7}$	0.000	0.000
X_{ssbb}	$-9.988\ 1\times10^{-7}$	0.000	0.000
X_{sbbb}	$-3.083\ 15\times10^{-7}$	0.000	0.000
X_{bbbb}	$-1.531\ 94\times10^{-7}$	0.000	0.000
k_{sbb}	−0.021 036 1	−0.021 012	0.000

$^{\text{a}}$Units cm^{-1}. All other parameters in units of ω_s.

$$X_{ssss}\to X_{ssss}c^{-4},\ldots, \tag{2.8d}$$

$$k_{sbb}\to k_{sbb}c^{-3/2}. \tag{2.8e}$$

We shall take $c=4$ in most of the quantum computations reported here (although see Sec. V C).

B. Classical Hamiltonian

Invoking the standard quantum-classical correspondence,[10] we can express the classical Hamiltonian corresponding to the quantum operator (2.7) in terms of two classical actionlike variables I_s and I_b and their conjugate angles ϕ_s and ϕ_b. For simplicity, we only consider explicitly the quadratic $\hat{H}^0$ case (i.e., vanishing cubic and quartic terms $\hat{H}_3^0$ and $\hat{H}_4^0$), for which

$$H=\omega_s I_s+\omega_b I_b+X_{ss}I_s^2+X_{sb}I_sI_b+X_{bb}I_b^2$$
$$+\frac{k_{sbb}}{\sqrt{2}}\,I_b\sqrt{I_s}\,\cos(\phi_s-2\phi_b). \tag{2.9}$$

Associated classical equations of motion are

$$\frac{dI_s}{dt}=-\frac{\partial H}{\partial\phi_s},\quad \frac{dI_b}{dt}=-\frac{\partial H}{\partial\phi_b},$$

$$\frac{d\phi_s}{dt}=\frac{\partial H}{\partial I_s},\quad \frac{d\phi_b}{dt}=\frac{\partial H}{\partial I_b}. \tag{2.10}$$

III. CLASSICAL PHASE SPACE STRUCTURE AND THE POLYAD PHASE SPHERE

In this section, following Li, Xiao and Kellman,[25] we review briefly the concept of the *polyad phase sphere* for Fermi resonant systems, and discuss the determination of periodic orbits and bifurcation structure.[25]

A. Transformation to phase sphere variables

The generating function[30]

$$F=(I+I_z)\phi_s+2(I-I_z)\phi_b \tag{3.1}$$

defines a canonical change of variables $(I_s,I_b,\phi_s,\phi_b)\to(I,I_z,\chi,\psi)$, where

$$I_s=(I+I_z),\quad I_b=2(I-I_z) \tag{3.2}$$

and

$$\chi=\phi_s+2\phi_b,\quad \psi=\phi_s-2\phi_b. \tag{3.3}$$

In terms of the new variables, the classical Hamiltonian (2.9) becomes

$$H=2\omega_0I+(P+QI)I_z+\alpha_1I^2+\alpha_2I_z^2$$
$$+k_{sbb}(I-I_z)\sqrt{2(I+I_z)}\cos\,\psi, \tag{3.4}$$

with

$$\omega_0=\tfrac{1}{2}(\omega_s+2\omega_b), \tag{3.5a}$$

$$P=(\omega_s-2\omega_b), \tag{3.5b}$$

$$Q=2X_{ss}-8X_{bb}, \tag{3.5c}$$

$$\alpha_1=X_{ss}+4X_{bb}+2X_{sb}, \tag{3.5d}$$

$$\alpha_2=X_{ss}+4X_{bb}-2X_{sb}. \tag{3.5e}$$

Note that Hamiltonian (3.4) is independent of the angle χ, so that the conjugate quantity I is a constant of the motion; conservation of $2I=(I_s+I_b/2)$ is the classical analog of the conservation of the polyad number P in the quantum case.

At fixed I, the dynamics of Hamiltonian (3.4) is best elucidated in terms of phase space coordinates on a *sphere*, the polyad phase sphere.[10] Coordinates on the sphere are the angle ψ conjugate to I_z, where $0\leq\psi\leq2\pi$, and the angle α, where

$$I_z=I\sin\,\alpha,\quad \frac{\pi}{2}\geq\alpha\geq-\frac{\pi}{2}. \tag{3.6}$$

B. Fixed points, periodic orbits, and bifurcations

Hamilton's equations of motion for I_z and ψ generate a vector field on the polyad phase sphere, and trajectories of the Hamiltonian (3.4) lie on contours of constant $H=E$ at fixed I. Kellman and co-workers have examined in considerable detail the correspondence between the form of eigenstates of quantum Hamiltonian (2.7) and the contours $H=E$ at the eigenvalue E.[10]

As the angle χ is a cyclic coordinate, the *stationary points* of the Hamiltonian on the sphere, i.e., those points for which

$$\frac{dI_z}{dt}=-\frac{\partial H}{\partial\psi}=0, \tag{3.7a}$$

$$\frac{d\psi}{dt}=\frac{\partial H}{\partial I_z}=0 \tag{3.7b}$$

correspond to *periodic orbits* in the full phase space. The location of periodic orbits can therefore be found by solving Eqs. (3.7). For Hamiltonian (3.4), condition (3.7a) becomes

$$k_{sbb}(I-I_z)\sqrt{2(I+I_z)}\sin\,\psi=0, \tag{3.8}$$

which is satisfied with $\psi=0$ or π. To find the associated values of I_z, Eq. (3.7b) must be solved

$$(P+QI)+2I_z\alpha_2\pm\sqrt{2}k_{sbb}\left[-\sqrt{I+I_z}+\frac{I-I_z}{2\sqrt{I+I_z}}\right]=0.$$

$$(3.9)$$

We solve this equation numerically.

In addition to the fixed points just described, there is a point of fixed action $I_z=I$ at the north pole of the polyad phase sphere; for this point the (finite) value of ψ is irrelevant. Hence, as noted by Li, Xiao, and Kellman,[25] all fixed points lie on a single great circle on the polyad phase sphere.

Once the location of the fixed point has been determined, the period of the corresponding periodic orbit can be calculated. For fixed points other than the north pole, the angular frequency Ω is

$$\Omega=\frac{\partial H}{\partial I}=2\omega_0+QI_z+2\alpha_1I\pm\sqrt{2}k_{sbb}\left[\sqrt{I+I_z}+\frac{I-I_z}{2\sqrt{I+I_z}}\right],$$

$$(3.10)$$

with the derivative evaluated at the fixed point. For the point of fixed action at the north pole,

$$\Omega=2\omega_0+P+2I(Q+\alpha_1+\alpha_2).\qquad(3.11)$$

In all cases the period τ corresponding to one cycle of the periodic motion associated with the fixed point is $\tau=4\pi/\Omega$.

By examining contours of the Hamiltonian H on the phase sphere at fixed I, we can determine whether a particular fixed point is elliptic (stable), hyperbolic (unstable), or a *cusp* (possible at the north pole[26]). As parameters such as coupling constants or the value of I are varied, the location of the fixed points will in general change. At a *bifurcation point*, the number and stability type of the fixed points can change. Xiao and Kellman have determined that for Fermi resonant Hamiltonians of the type discussed here there are four distinct *zones* corresponding to four basic patterns of fixed points on the sphere, and have exhibited a catastrophe map that locates points in parameter space in one of the four zones.[26]

For the classical-quantum analysis to follow, we are interested in the form of the bifurcation diagram obtained by varying the action I. In Fig. 1, we show the location of the fixed points as a function of I for the resonant Hamiltonian H^{res} as I is varied from 0.5 to 5.5 (covering a range of energy approximately $1.0\rightarrow11.0$). At small I, there are two stable fixed points, one at the north pole and one near the south pole; this is zone I (nonresonant) in Xiao and Kellman's classification.[26] As I increases, a bifurcation occurs in which the point of fixed action at the north pole becomes a cusp, and a stable fixed point moves off the north pole along the line $\psi=\pi$. The system is now in zone II. As I increases further, the cusp at the north pole bifurcates again, becoming a stable fixed point, and shedding an unstable fixed point which moves away from the pole along the line $\psi=0$. The system phase sphere now has four fixed points, and lies in zone III of Xiao and Kellman's scheme. Finally, the stable and unstable fixed points on the line $\psi=0$ merge in an in-
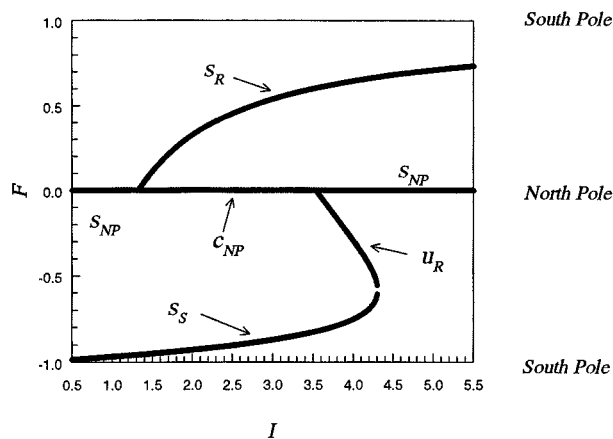

FIG. 1. Classical bifurcation diagram for the resonant fitting Hamiltonian H^{res} showing the location of fixed points (F) vs action I. The function $F=-(I-I_z)\cos\psi/2I$, where I_z is the value of $1/2(I_s-I_b/2)$ at the fixed point, and $\psi=0$ or π. The point of fixed action at the north pole has $F=0$.

verse saddle-center bifurcation, and the system passes from zone III to zone IV, where the latter is a nonresonant region of phase space with two stable fixed points. The evolution of the phase space structure described here is very similar to that found for the resonant Hamiltonian for HC(CF$_3$)$_3$ studied in Ref. 27. By contrast, the phase sphere for the diagonal fitting Hamiltonian $\hat{H}^{diag}$ exhibits no bifurcations.

For each of the fixed points in Fig. 1 we can determine the energy E and period τ of the associated periodic orbit. The resulting classical (E,τ) plot is shown in Fig. 2. The evolution of the phase space structure with E (rather than I) is readily apparent; the inverse saddle-center bifurcation marking the passage from zone III to zone IV is particularly prominent.

In the following sections, we show how the quantum (E,τ) plot obtained by Gabor transform analysis of the quantum spectrum[19] reflects the full classical bifurcation structure.
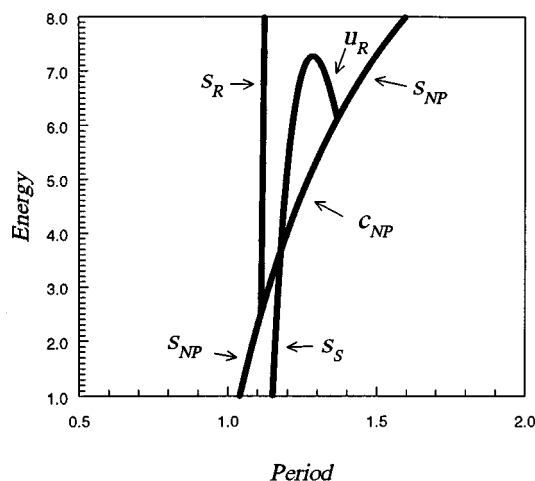

FIG. 2. Classical (E,τ) plot for fundamental periodic orbits of the resonant fitting Hamiltonian $\hat{H}^{res}$. Periods τ are measured in units of 2π.

IV. PERIODIC ORBIT ANALYSIS OF QUANTUM DENSITY OF STATES

In this section, we briefly review the basic results of semiclassical periodic orbit (po) theory,[1,2] and describe the Gabor transform technique[19] used to analyze the quantum density of states for Fermi resonant systems (see also Refs. 20–23).

A. Semiclassical periodic orbit sums

The key result of semiclassical periodic orbit theory is an approximate expression for the density of states at energy E, $n(E) = \Sigma_i \delta(E - E_i)$, in the limit $\hbar \rightarrow 0$ as a smooth term (Thomas–Fermi) plus a sum of oscillatory contributions from classical pos and their repetitions

$$n(E) \simeq \bar{n}(E) + \sum_p \sum_k A_{pk}(E)$$

$$\times \exp\left\{ i \left[\frac{2\pi k S_p(E)}{\hbar} + \phi_{pk} \right] \right\}. \qquad (4.1)$$

Here, the subscript p specifies the po and the index k labels its kth repetition. The quantity $\bar{n}(E)$ is the mean level density, and is a smooth function of the energy E. The oscillatory part of the density of states is then a sum of contributions from all pos p. The quantity S_p in the exponent is the action of po p. The precise form of the amplitude A_{pk} depends on the nature of the system phase space in the vicinity of po p, while ϕ_{pk} is an unimportant (for present considerations) phase. Both S_p and A_{pk} depend on the energy E in general.

Consider first the integrable case. For an integrable system, phase space is filled with invariant tori,[2] and the semiclassical density of states can be computed using the EBK quantization condition.[31] In this case, a version of the semiclassical po sum (4.1) due to Berry and Tabor expresses the density of states as a sum of contributions from rational or periodic *tori*.[4]

In integrable systems with 2 degrees of freedom, pos typically appear in continuous 1-parameter families (at fixed energy) covering rational tori. In completely (harshly) chaotic systems, all pos are unstable and isolated (fixed E).[1] Moreover, upon perturbation of an integrable system by a nonintegrable coupling term, the continuous families of (the least irrational) rational orbits will in general disappear, leaving pairs of isolated stable and unstable pos (resonant island chains[2]). For the completely chaotic case and also for the case of "large" resonant islands (island area $\gg \hbar$), the Gutzwiller trace formula (GTF)[1] expresses the quantum mechanical density of states as a sum over isolated periodic orbits. In the primitive semiclassical version of the GTF, the magnitude of the amplitude A_{pk} depends on the linearized dynamics in the vicinity of the po p.[1,2]

The amplitudes for stable pos diverge at bifurcation points, where the stationary phase approximations used in the derivation of the GTF break down.[2] Uniform semiclassical approximations that yield finite amplitudes near and at classical bifurcation points have been developed[32] and applied.[33,34]

It is important to note the $\hbar$ dependence of the various contributions to the semiclassical density of states. For a 2-mode systems, the Thomas–Fermi density of states is proportional to $\hbar^{-2}$. The amplitudes for isolated pos (GTF) go as $\hbar^{-1}$, whereas the contribution to the density of states from a continuous family of pos (Berry–Tabor) is proportional to $\hbar^{-3/2}$. Hence, as $\hbar \rightarrow 0$, the contributions to the density of states from families of pos (rational tori) are larger by a factor $\hbar^{-1/2}$ than those from isolated pos.

A discussion of the relation between the Berry–Tabor formula and the GTF po sum for a system passing from the small resonant island to the large island limit has been given by Ozorio de Almeida.[2,5]

Although the semiclassical po expressions for the level density can in principle be used to compute semiclassical eigenvalues, in practice there are many difficult fundamental issues concerning enumeration of pos and convergence, especially for systems such as molecular Hamiltonians that exhibit typical "mixed" phase space structure with both regular and chaotic regions present.[35]

In the present paper we use semiclassical po theory "in reverse" to extract information on classical phase space structure directly from the vibrational eigenvalues, and so avoid these fundamental convergence issues. The connection between fluctuations of the quantum density of states about the mean (Thomas–Fermi) value and classical pos is revealed by Fourier transformation of the quantum spectrum, whose power spectrum will exhibit peaks at multiples of the periods (or actions) of the least unstable pos.[1] This approach has been applied to several problems, including the hydrogen atom in a magnetic field,[6] model two-electron systems,[7] coupled quartic oscillators,[9] and the absorption spectrum of the O_3 molecule.[17]

To examine the correspondence between the numerical Fourier transform of the density of states and the properties of classical pos, we construct plots of po period τ vs energy E directly from the quantum spectrum, and compare the results with the corresponding classical mechanical results.

B. Gabor transform of the density of states

For scaling systems (i.e., systems with potential functions homogeneous in coordinates) the classical phase space structure is effectively independent of energy,[1] which greatly facilitates study of the classical-quantum correspondence via semiclassical po theory.[6,7,9]

In nonscaling systems, such as typical molecular vibrational Hamiltonians, the phase space structure has a nontrivial E dependence, as do the po actions, periods and stability parameters. Indeed, it is just this E dependence of the dynamics which gives molecular vibrational Hamiltonians much of their interest.[12] To obtain information on the classical dynamics from the quantum spectrum, it is then necessary to analyze the density of states in the vicinity of a particular energy value $\bar{E}$. One obvious possibility is to multiply

the density of states by a suitable *window function* centered at $\bar{E}$.

A windowed Fourier transform of the absorption spectrum of O_3 was used by Johnson and Kinsey to examine the evolution of po periods with energy on the dissociative upper potential energy surface.[17] The window used was a three-term Blackman–Harris function.[16] Baranger *et al.* have shown more formally that the Fourier transform of the quantum density of states with respect to E obtained using a Gaussian window centered at some chosen energy $\bar{E}$ contains peaks associated with classical pos at the same chosen energy.[19] Use of a Gaussian window of width ΔE corresponds to taking the *Gabor transform* of the density of states[14]

$$G_{\bar{E}}(t) = \int_{-\infty}^{\infty} \exp\left[-\frac{(E-\bar{E})^2}{2\Delta E^2}\right] \exp\left(\frac{-iEt}{\hbar}\right) \text{Tr}[\delta(E-\hat{H})]dE$$

$$= \sum_n \exp\left[-\frac{(E_n-\bar{E})^2}{2\Delta E^2}\right]\exp\left(\frac{-iE_n t}{\hbar}\right). \qquad (4.2)$$

The power spectrum is then simply $|G_{\bar{E}}(t)|^2$. In the semiclassical limit $\hbar \to 0$, we can substitute the GTF for the density of states into Eq. (4.2); after expanding the E-dependent po action about $\bar{E}$, noting that the po period

$$\tau_p = \frac{\partial S_p(E)}{\partial E}, \qquad (4.3)$$

and ignoring the E dependence of the amplitudes A_{pk}, we obtain a power spectrum with peaks centered at the *periods* τ_p of classical pos at the energy $\bar{E}$. Computation of the power spectrum $|G_{\bar{E}}(t)|^2$ at many values of $\bar{E}$ yields an energy versus period (E, τ) plot, which can be compared with the corresponding classical result.[17,19]

In the next section we present quantum (E, τ) plots for the Fermi resonant Hamiltonians of Sec. II, and compare with the classical mechanical results of Sec. III.

V. QUANTUM (E, τ) PLOTS FOR FERMI RESONANT SYSTEMS

A. Quantum (E, τ) plots: Qualitative aspects

In Fig. 3 we show quantum (E, τ) plots calculated for the three Hamiltonians defined in Sec. II. The energy range is from $E=1.0$ to $E=8.0$, while the τ range goes from 0.5 to 5.5 (units of 2π). The latter range covers the first four repetitions of the fundamental pos.

Figure 3(a) shows the (E, τ) plot for the reference Hamiltonian $\hat{H}^{\text{sim}}$. A key aspect of this plot is the looplike feature between $E\sim 4.5$ and $E\sim 7.0$. This feature occurs for each multiple of the fundamental po periods, and is most clearly seen at the third repetition. Figure 3(b) shows the corresponding plot for the resonant fitting Hamiltonian $\hat{H}^{\text{res}}$. It is immediately apparent that the (E, τ) plots for $\hat{H}^{\text{sim}}$ and $\hat{H}^{\text{res}}$ are remarkably similar. In particular, the looplike feature is present in both plots. We show in the next subsection that this looplike feature is a direct manifestation of po bifurcations and mergings on the polyad phase sphere (cf. Fig. 2).
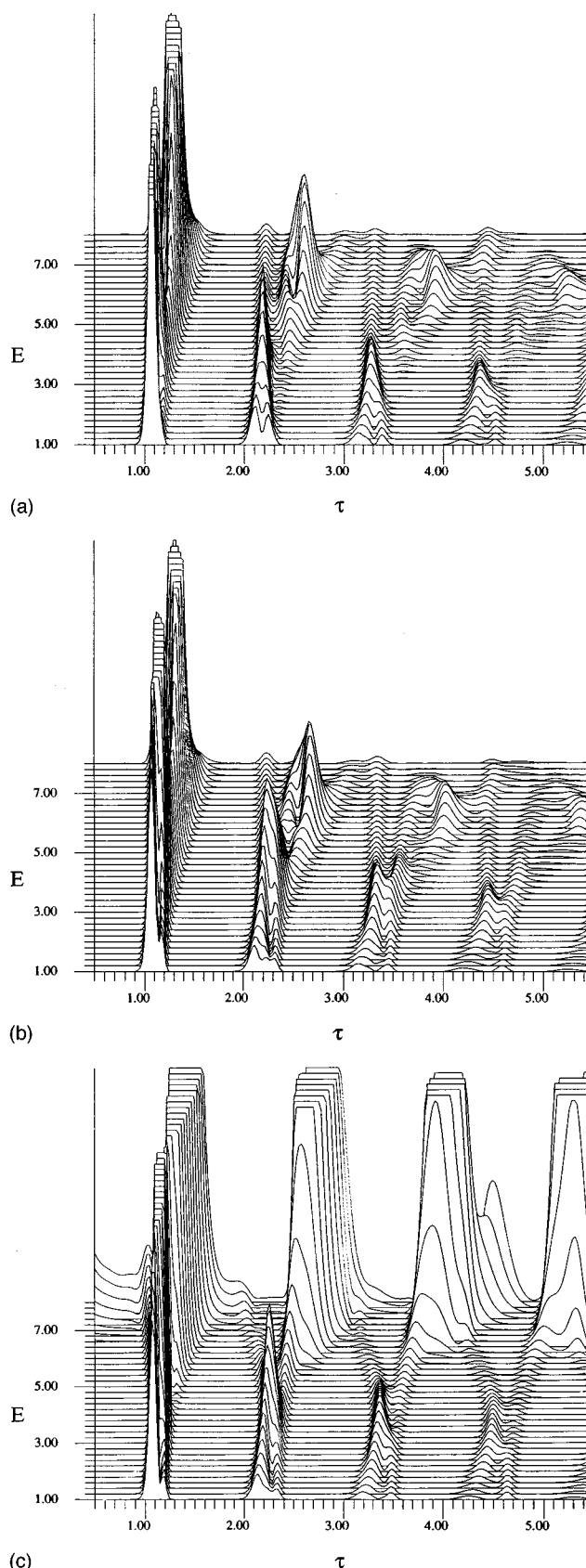

FIG. 3. Quantum (E, τ) plots computed for Fermi resonant Hamiltonians. (a) Full Hamiltonian $\hat{H}^{\text{sim}}$; (b) resonant fitting Hamiltonian $\hat{H}^{\text{res}}$; (c) diagonal fitting Hamiltonian $\hat{H}^{\text{diag}}$.

Figure 3(c) shows the (E,τ) plot for the diagonal fitting Hamiltonian $\hat{H}^{\mathrm{diag}}$. With no further analysis whatsoever, it is quite obvious that, even at the relatively low level of resolution associated with the τ range examined here, the level structure of $\hat{H}^{\mathrm{diag}}$ is qualitatively different from those of $\hat{H}^{\mathrm{sim}}$ and $\hat{H}^{\mathrm{res}}$.

The quantum (E,τ) plot is therefore, at the most rudimentary level, a very efficient tool for comparing "spectral patterns"[24] inherent in level structures associated with different Hamiltonians. Although the different spectral patterns seen for the resonant and diagonal Fermi Hamiltonians can be correlated with differences in classical phase space structure, the quantum (E,τ) plots immediately reveal qualitative differences between spectra without the necessity of either a detailed study of the underlying classical mechanics or an exhaustive level-by-level comparison of spectra.

Svitak *et al.* have recently analyzed level spacings in polyads of 2:1 resonantly coupled modes, and have noted that the presence of a separatrix in the classical phase space is signalled by the existence of a "dip" in ΔE vs E plots, which is associated with the vanishing of one classical frequency on the separatrix.[24] Both the Hamiltonians $\hat{H}^{\mathrm{sim}}$ and $\hat{H}^{\mathrm{res}}$ have separatrices on their classical phase spheres in the range of energy studied here, whereas the diagonal Hamiltonian $\hat{H}^{\mathrm{diag}}$ does not, due to the absence of a resonant coupling term.[24] Recognizing the presence of such characteristic patterns using the approach of Svitak *et al.* becomes difficult, however, as the spectrum becomes more complicated. The periodic orbit analysis presented here is a systematic device for revealing patterns (correlations) in the level density. The connection with the analysis of Svitak *et al.* is as follows: The dip in the level spacing due to the presence of a separatrix leads to a local increase in the density of states for a single polyad, i.e., a bunching of levels. Superposition of level densities for successive polyads results in a modulation of the density of states due to the bunching; this modulation manifests itself in the power spectrum of the density of states as a peak at the period of the *unstable* periodic orbits whose stable and unstable manifolds define the separatrix. Of course, the (E,τ) analysis of the spectrum also reveals many other correlations in the spectrum whose existence is not obvious upon inspection of the energy levels.

B. Classical-quantum correspondence for Fermi Hamiltonians

In this subsection we examine in more detail the classical-quantum correspondence for the Fermi Hamiltonians $\hat{H}^{\mathrm{diag}}$ and $\hat{H}^{\mathrm{res}}$.

1. Diagonal Hamiltonian $\hat{H}^{diag}$

The diagonal Hamiltonian

$$\hat{H}^{\mathrm{diag}} = \hat{H}_2^0 + \hat{H}_3^0 \tag{5.1}$$

is a sum of quadratic and cubic terms [see Eqs. (2.2) and (2.3)], and conserves the zeroth-order quantum numbers n_s and n_b. The parameters for $\hat{H}^{\mathrm{diag}}$ are listed in Table I, and
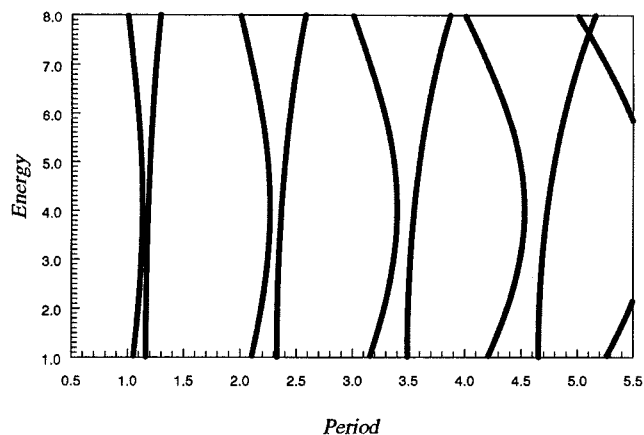

FIG. 4. Classical (E,τ) plot for the diagonal fitting Hamiltonian $\hat{H}^{\mathrm{diag}}$.

were determined by Svitak *et al.* by least-squares fit to the levels of $\hat{H}^{\mathrm{sim}}$ for polyads 1–6 (n_b even; cf. Table II of Ref. 24).

In terms of the polyad phase sphere, the phase space structure of the classical Hamiltonian H^{diag} is very simple. There is a point of fixed action at the north pole, which corresponds to a stable po with all the energy in the stretching mode, and a fixed point at the south pole, corresponding to the stable po with all energy in the bending mode. There are no other fixed points and, in particular, no separatrix dividing motion of one kind from another. At fixed $2I = I_s + I_b/2$, the phase sphere is covered by a continuous 1-parameter family of invariant curves, each associated with an action pair (I_s, I_b). Frequencies of the polar pos are

$$\Omega_s = \omega_s + 2X_{ss}I_s + 3X_{sss}I_s^2, \tag{5.2a}$$

$$\Omega_b = 2\{\omega_b + 2X_{bb}I_b + 3X_{bbb}I_b^2\}. \tag{5.2b}$$

An E vs τ plot for these polar pos and their second, third, and fourth repetitions is shown in Fig. 4. Comparison with Fig. 3(c) clearly shows the traces of the polar pos in the quantum (E,τ) plot. There are additional large peaks present in Fig. 3(c). These peaks are associated with contributions to the level density from families of rational tori[4] (cf. our study of the 1:1 resonant case[20]). Further analysis of these resonant peaks is complicated in the present case by the fact that the contours of H^{diag} in (I_s, I_b) action space are very flat. Moreover, the frequency ratio $\rho = \Omega_s/2\Omega_b$ can vary nonmonotonically at fixed E as the fraction of energy in the stretching mode is changed. Quantitative analysis of the density of states therefore requires a uniform semiclassical analysis,[4] which we do not pursue here.

2. Resonant Hamiltonian $\hat{H}^{res}$

A classical (E,τ) plot showing the periods of the fundamental pos for the resonant Hamiltonian H^{res} and their repetitions as a function of energy is given in Fig. 5 (cf. Fig. 2). Comparison with Fig. 3(c) shows that the looplike feature in the quantum (E,τ) plot is a direct manifestation of the sequence of po bifurcations and mergings on the phase sphere discussed in Sec. III.
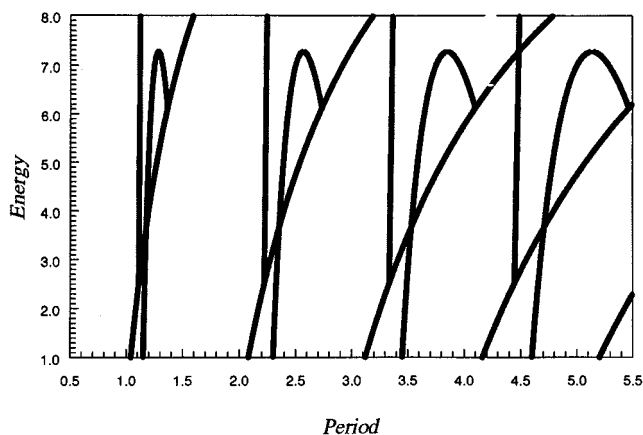
FIG. 5. Classical (E,τ) plot for the resonant fitting Hamiltonian $\hat{H}^{\text{res}}$.

FIG. 6. Quantum (E,τ) plot for the resonant Hamiltonian $\hat{H}^{\text{res}}$ with $\hbar = 1/2$.

At energies below $E \sim 2.5$, there are two stable pos, s_{NP} and s_S, and the system is in zone I.[26] At $E \sim 2.5$, the point of fixed action at the north pole bifurcates to give a cusp at the pole (c_{NP}) and a stable fixed point off the pole (s_R). The system is now in zone II. At $E \sim 6.2$, the fixed point c_{NP} bifurcates again to yield a stable po at the pole (s_{NP}) and an unstable po off the pole (u_R). The system is now in zone III, and we have two stable pos (s_S and s_{NP}) and a stable/unstable pair (s_R and u_R). The stable/unstable pair (s_R,u_R) define a pendular resonance zone as in the usual Chirikov picture.[36] Finally, at $E \sim 7.3$, the pos u_R and s_S annihilate each other in an inverse saddle-center bifurcation, leaving the two stable pos s_{NP} and s_R. The system is now in the nonresonant zone IV.[26] It is remarkable that the complicated evolution of phase space structure just described can be followed in full detail in the quantum (E,τ) plot for $\hat{H}^{\text{res}}$.

The looplike structure appearing in Figs. 3(a) and 3(b) is a motif that is characteristic of Fermi resonant Hamiltonians of the kind studied here; this structure appears, for example, in the (E,τ) plots for the stretch–bend Hamiltonian for CH(CF$_3$)$_3$.[37]

C. Increasing $\hbar$: Moving out of the semiclassical regime

All quantum calculations discussed so far were carried out using an effective value of $\hbar = 1/4$ [cf. Eq. (2.8)]. Specifically, 861 energy levels corresponding to all integer values of polyad quantum number P between 0 and 40 were used in computing the quantum (E,τ) plots shown in Fig. 3. Although far from the true semiclassical limit, this value of $\hbar$ enables one to resolve quite clearly the detailed po bifurcation pattern in the (E,τ) plots.

We now examine the effect of increasing the value of $\hbar$; i.e., we move away from the semiclassical limit. In Fig. 6, we show the quantum (E,τ) plot for $\hat{H}^{\text{res}}$ computed with $\hbar = 1/2$. Specifically, 231 levels corresponding to all integer values of P between 0 and 20 were used to compute the (E,τ) plot; with the parameter scalings of Eq. (2.8), these levels span the same energy range as the 861 levels obtained
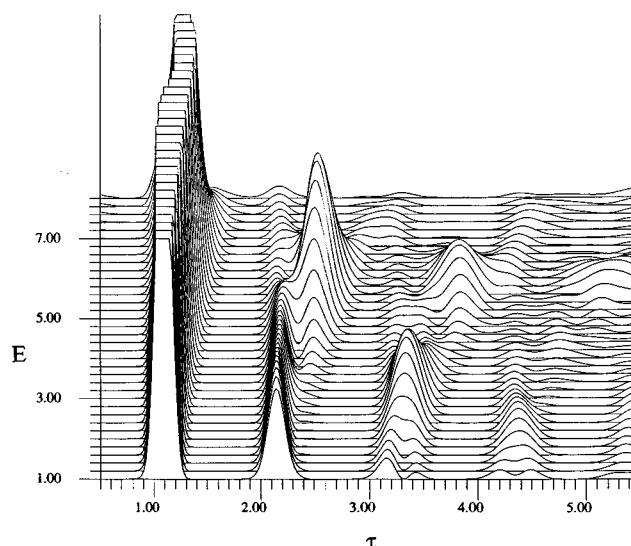
with $\hbar = 1/4$. Although some of the fine detail is lost, the characteristic ''loop'' seen in Figs. 3(a) and 3(b) is still clearly present.

In Fig. 7 we show three quantum (E,τ) plots computed with $\hbar = 1$. This is the physical value of $\hbar$, and corresponds to a situation very far from the semiclassical limit: Only 67 levels now span the whole energy range of interest, corresponding to all integer values of P from 0 to 10. Two points can be made. First, most of the detail of the classical po bifurcation structure is lost for this value of $\hbar$; only a hint of the formerly resolved structure remains. Nevertheless, it is still true that the (E,τ) plots serve to distinguish immediately between the spectra of $\hat{H}^{\text{sim}}$ and $\hat{H}^{\text{res}}$ on the one hand [Figs. 7(a) and 7(b)], and that of $\hat{H}^{\text{diag}}$ on the other [Fig. 7(c)].

VI. CONCLUSIONS

In this paper we have applied semiclassical periodic orbit theory to analyze the quantum density of states for three model molecular vibrational Hamiltonians describing stretch/bend modes with and without 2:1 (Fermi) resonant coupling.[24] Periods of classical periodic orbits as a function of energy are extracted directly from the quantum spectrum using a Gaussian windowed (Gabor) Fourier transform.[19] The quantum (E,τ) plots so obtained provide an extremely informative representation of the level structure (cf. also Refs. 21 and 22). At a qualitative level, similarities and differences between spectra (i.e., resonant vs nonresonant coupling) are immediately apparent; in this sense, the quantum (E,τ) plot is an efficient device for recognition and analysis of spectral patterns. At a more detailed level of analysis, for sufficiently small effective values of $\hbar$, the quantum (E,τ) plot reflects in full detail the intricate periodic orbit bifurcation structure for Fermi resonant Hamiltonians previously elucidated by Li et al.[25] In particular, passage of the system between different zones[26,27] can be seen directly in the quantum (E,τ) plot.
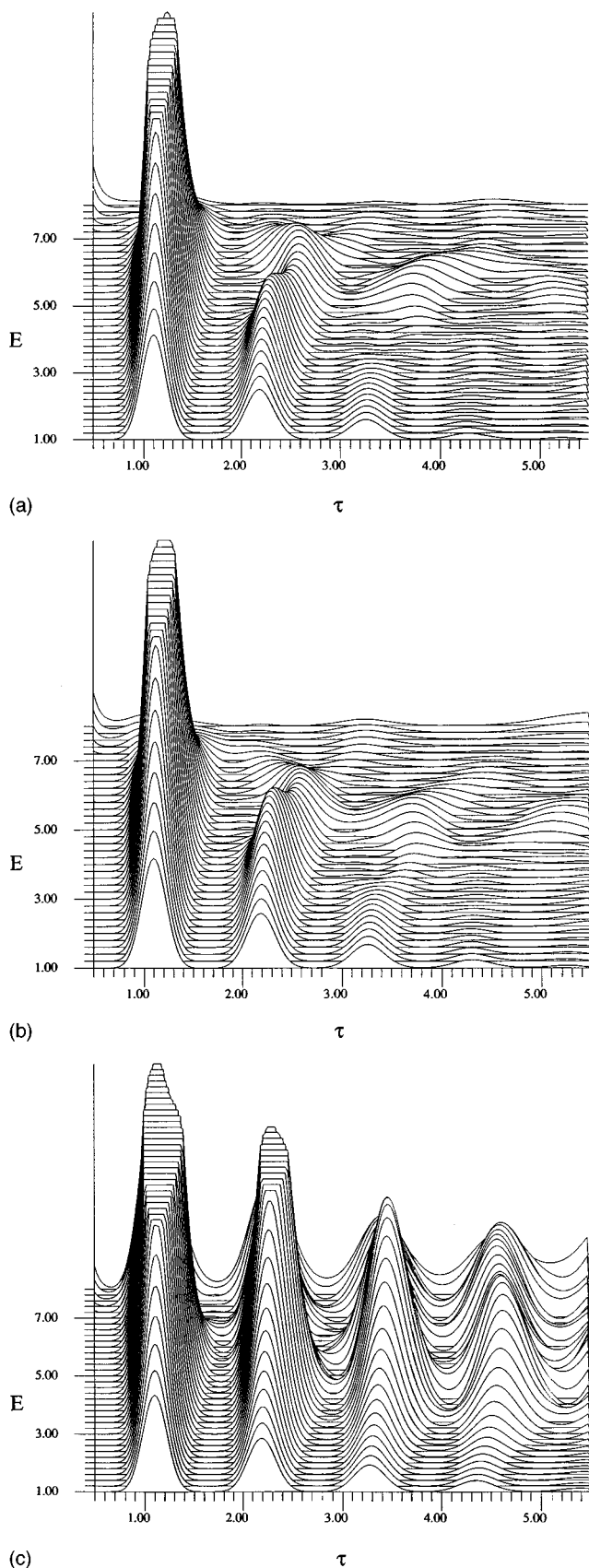
(a)

(b)

(c)

FIG. 7. Quantum (E,τ) plots computed for Fermi resonant Hamiltonians. $\hbar=1$. (a) Full Hamiltonian $\hat{H}^{sim}$; (b) resonant fitting Hamiltonian $\hat{H}^{res}$; (c) diagonal fitting Hamiltonian $\hat{H}^{diag}$.

Our work in this and a previous paper[20] has established the utility of the quantum (E,τ) (or "vibrogram," cf. Refs. 21 and 22) representation of the level spectrum in revealing po bifurcation patterns associated with abrupt changes in the underlying classical phase space structure with energy. Some additional comments are in order. First, we note that there are close connections between the quantum (E,τ) analysis presented here and the hierarchical tree approach of Davis.[11,38] As already pointed out by Davis (Ref. 38, Sec. 3.2.1), the hierarchical tree structure can be used to simplify analysis of recurrences in wave packet autocorrelation functions. The tree analysis provides a set of square (in energy) windows associated with groups of states grouped in subtrees.[11] The connection with semiclassical po theory has not, however, been stressed by Davis. In this connection it must be noted that analysis of the classical-quantum correspondence via po theory requires that the effective value of $\hbar$ be sufficiently small. In the present work, the value $\hbar=1/4$ is small enough to enable fine details of the po τ vs E traces to be resolved. As $\hbar$ is increased to its physical value ($\hbar=1$), much of the fine structure of the (E,τ) plot is washed out. This is hardly surprising, as there are only 67 states in all over the whole energy range of interest for $\hbar=1$. Nevertheless, the quantum (E,τ) plot still serves to distinguish resonant and nonresonant Hamiltonians, and in the resonant case traces of the bifurcation structure seen at smaller $\hbar$ can still be seen.

The systems studied in this work and in our previous paper are both 2-mode vibrational Hamiltonians with a single resonant coupling term, and are therefore classically integrable. Now that we have studied the details of the manifestations of resonant bifurcations due to isolated 1:1 and 1:2 couplings, we can proceed to investigate manifestations of nonintegrability in the (E,τ) plot when two coupling terms are present. Work on this problem is in progress.[37]

ACKNOWLEDGMENTS

[1] M. Gutzwiller, *Chaos in Classical and Quantum Mechanics* (Springer, Berlin, 1990).

[2] A. M. Ozorio de Almeida, *Hamiltonian Systems: Chaos and Quantization* (Cambridge University, London, 1988).

[3] W. H. Miller, J. Chem. Phys. **56**, 38 (1972); **63**, 996 (1975).

[4] M. V. Berry and M. Tabor, Proc. R. Soc. London, Ser. A **349**, 101 (1976).

[5] A. M. Ozorio de Almeida, Lect. Notes Phys. **263**, 197 (1986).

[6] H. Friedrich and D. Wintgen, Phys. Rep. **183**, 37 (1989).

[7] J. H. Kim and G. S. Ezra, in *Proc. Adriatico Conf. Quantum Chaos*, edited by H. A. Cerdeira, R. Ramaswamy, M. C. Gutzwiller and G. Casati (World Scientific, Singapore, 1991).

[8] D. Wintgen, K. Richter, and G. Tanner, CHAOS **2**, 19 (1992).

[9] B. Eckhardt, G. Hose, and E. Pollak, Phys. Rev. A **39**, 3776 (1989); G. G. de Polavieja, F. Borondo, and R. M. Benito, Phys. Rev. Lett. **73**, 1613 (1994); K. M. Atkins and G. S. Ezra, Phys. Rev. E **51**, 1822 (1995).

[10] M. E. Kellman, in *Molecular Dynamics and Spectroscopy by Stimulated Emission Pumping*, edited by H.-L. Dai and R. W. Field (World Scientific, Singapore, 1995).

[11] M. J. Davis, Chem. Phys. Lett. **192**, 479 (1992); J. Chem. Phys. **98**, 2614 (1993); in *Molecular Dynamics and Spectroscopy by Stimulated Emission Pumping*, edited by H.-L. Dai and R. W. Field (World Scientific, Singapore, 1995).

[12] J. M. Gomez Llorente, S. C. Farantos, O. Hahn, and H. S. Taylor, J. Opt. Soc. B **7**, 1851 (1990); R. Schinke, K. Weide, B. Heumann, and V. Engel, Faraday Discuss. Chem. Soc. **91**, 31 (1991); J. M. Gomez Llorente and E. Pollak, Annu. Rev. Phys. Chem. **43**, 91 (1992); S. C. Farantos, in *Time-dependent Molecular Quantum Dynamics*, edited by J. Broeckhove and L. Lathouwers (Plenum, New York, 1992).

[13] E. J. Heller, in *Chaos in Quantum Physics*, edited by M.-J. Giannoni, A. Voros, and J. Zinn-Justin, (Elsevier, New York, 1991); M. A. Sepulveda and E. J. Heller, J. Chem. Phys. **101**, 8004, 8016 (1994).

[14] D. Gabor, J. Inst. Electr. Eng. (London) **93**, 429 (1946).

[15] C. C. Martens, M. J. Davis, and G. S. Ezra, Chem. Phys. Lett. **142**, 519 (1987).

[16] F. J. Harris, Proc. IEEE **66**, 51 (1978).

[17] B. R. Johnson and J. L. Kinsey, J. Chem. Phys. **91**, 7638 (1989). See also O. Zobay and G. Alber, J. Phys. B **26**, L539 (1993).

[18] K. Husimi, Proc. Phys.-Math. Soc. Jpn **22**, 264 (1940).

[19] M. Baranger, M. R. Haggerty, B. Lauritzen, D. C. Meredith, and D. Provost, CHAOS **5**, 261 (1995); see also E. J. Heller and S. Tomsovic, in *Coherent States: Past, Present and Future*, edited by D. Feng, J. R. Klauder, and M. Strayer (World Scientific, Singapore, 1994).

[20] D. C. Rouben and G. S. Ezra, J. Chem. Phys. **103**, 1375 (1995).

[21] J. Liévin, M. Abbouti Temsamani, P. Gaspard, and M. Herman, Chem. Phys. **190**, 419 (1995).

[22] K. Hirai, E. J. Heller, and P. Gaspard, J. Chem. Phys. **103**, 5970 (1995).

[23] P. O'Connor and M. E. Kellman (private communication).

[24] J. Svitak, Z. Li, J. Rose, and M. E. Kellman, J. Chem. Phys. **102**, 4340 (1995).

[25] Z. Li, L. Xiao, and M. E. Kellman, J. Chem. Phys. **92**, 2251 (1990).

[26] L. Xiao and M. E. Kellman, J. Chem. Phys. **90**, 6086 (1989).

[27] L. Xiao and M. E. Kellman, J. Chem. Phys. **93**, 5805 (1990).

[28] H. R. Dübal and M. Quack, J. Chem. Phys. **81**, 3775 (1984).

[29] D. Papousek and A. R. Aliev, *Molecular Vibrational-Rotational Spectra* (Elsevier, New York, 1982).

[30] H. Goldstein, *Classical Mechanics* (Addison-Wesley, Reading, MA, 1980).

[31] I. C. Percival, Adv. Chem. Phys. **XXXVI**, 1 (1977).

[32] A. M. Ozorio de Almeida and J. H. Hannay, J. Phys. A **20**, 5873 (1987).

[33] M. Kuś, F. Haake and D. Delande, Phys. Rev. Lett. **71**, 2167 (1993); M. W. Biems and G. Alber, Phys. Rev. A. **48**, 3123 (1993).

[34] K. M. Atkins and G. S. Ezra, Phys. Rev. A **50**, 93 (1994).

[35] See *Chaos and Quantum Physics*, edited by M.-J. Giannoni, A. Voros, and J. Zinn-Justin (Elsevier, New York, 1991); *Quantum Chaos*, Proc. Intl. School Phys. ''Enrico Fermi'' (North-Holland, Amsterdam, 1993).

[36] B. V. Chirikov, Phys. Rep. **52**, 263 (1979).

[37] G. S. Ezra (unpublished).

[38] M. J. Davis, Int. Rev. Phys. Chem. **14**, 15 (1995).